Investigation of anomalous hydrogen evolution from anodized magnesium using a polarization routine for scanning electrochemical microscopy

D. Filotás[1,2], B.M. Fernández-Pérez[3], L. Nagy[1,2], G. Nagy[1,2,*], R.M. Souto[3,4,*]

[1] *Department for General and Physical Chemistry, Faculty of Sciences, University of Pécs, Ifjúság útja 6, 7624 Pécs, Hungary.*

[2] *János Szentágothai Research Center, University of Pécs, Ifjúság u. 20, Pécs, 7624 Hungary.*

[3] *Department of Chemistry, Universidad de La Laguna, Avda. Astrofísico Francisco Sánchez s/n, E-38205 La Laguna (Tenerife), Canary Islands, Spain.*

[4] *Institute of Material Science and Nanotechnology, Universidad de La Laguna, P.O. Box 456, E-38200 La Laguna (Tenerife), Canary Islands, Spain.*

Abstract

With the goal to facilitate a new experimental procedure for the monitoring of anomalous hydrogen evolution from anodically-polarized magnesium-based materials, this paper presents the application of the three-step (off-on-off) anodization operation sequence for amperometric scanning electrochemical microscopy (SECM) recently by our group to the characterization of 99.9% magnesium in aqueous saline solution. The SECM measurements done above prepolarized and nonpolarized magnesium provided new information on the hydrogen evolution reaction (HER) on this metal, whereas other experiments are presented that enable to monitor the effect of the oxy-hydroxide layer formed on the metal under anodic polarization. In addition, direct comparison of the data obtained for 99.9% magnesium with those previously obtained for AZ63 magnesium alloy contributed to separate the effect of noble impurities from the catalytic effect of the oxy-hydroxide layer formed on magnesium for the hydrogen-evolution reaction.

Keywords: anodic polarization; anomalous hydrogen evolution; corrosion; magnesium; scanning electrochemical microscopy.

Corresponding authors: Ricardo M. Souto, Department of Chemistry, Universidad de La Laguna, P.O. Box 456, E-38200 La Laguna, Tenerife, Canary Islands, Spain.
E-mail: rsouto@ull.es; Tel: +34 922 318067.

Géza Nagy, Department for General and Physical Chemistry, Faculty of Sciences, University of Pécs, Ifjúság útja 6, 7624 Pécs, Hungary.
E-mail: g-nagy@gamma.ttk.pte.hu.

1. Introduction

A 3-step polarization procedure for amperometric scanning electrochemical microscopy (SECM) was recently developed by our group for the investigation of anomalous hydrogen evolution from highly reactive metals and alloys exposed to aqueous environments was [1]. While the proof of concept and presented data were related to the hydrogen evolution reaction (HER) on a particular magnesium alloy [1], AZ63, that was purposely chosen due to its lower hydrogen evolution rates compared to magnesium in dilute chloride-containing solution, this work focuses on pure magnesium (actually 99.9 % purity Mg). In addition to gaining insights on the HER on the pure metal and the influence of oxy-hydroxide layers formed on the surface, the proposed methodologies allows us to compare the findings for 99.9% magnesium with those obtained for the AZ63 alloy.

One of the hottest topics today in Corrosion Science is the quest to come up with a satisfactory explanation for the higher rate of the hydrogen evolution reaction (HER) that occurs in anodically polarized magnesium-based materials (often referred as the negative difference effect, NDE, or more strictly anomalous hydrogen evolution). Contrary to Butler-Volmer theory, which suggests that the rate of the H_2 evolution should decrease exponentially as the applied potential becomes more anodic, a linear increase is found [2]. Despite the extensive literature generated on this "anomalous effect", until now no consensus has been reached to justify it, and different and often contradictory mechanisms can be found in the literature as reported in various exhaustive reviews [3-5]. In particular, experimental challenges focus on ascertaining the actual effect of the oxy-hydroxide layers formed on the surface of the material in aqueous environment, as to whether they would passivate the surface or rather exhibit a catalytic effect towards HER [6-8], as well as the role of more noble alloying elements and impurities on this reaction as they might operate as local cathodes in the corrosion cell [9-11]. Therefore, the experimental strategies presented in this work were especially developed to address these two particular contributions to the corrosion mechanism of magnesium-based materials using SECM.

Since corrosion is an electrochemical process, electrochemical techniques are very popular in corrosion testing in general, and for research on the corrosion of magnesium and its alloys in particular. But it should be noted that the HER on magnesium does not obey the Faraday's law, so the exclusive use of electrochemical methods is not enough to assess the amount of dissolved magnesium. In other words, a fraction of the electrons produced under anodic polarization will not pass through the potentiostat but will be consumed by the HER. In potentiodynamic polarization measurements, the potential of the sample is scanned with

respect to a reference electrode at a constant scanning rate and the current is measured, the latter being determined by the relative rates of anodic and cathodic reactions. In the case of the Mg electrode, the increase in potential is accompanied by a strong increase in the anodic current, that is to say that the magnesium is non-polarizable. It should be noted that the potential drop caused by the formation of hydrogen bubbles interferes with a reliable analysis. The evolution of hydrogen at high anodic potentials cannot be properly described using standard electrochemical kinetics of the activation-controlled reactions. Therefore, galvanostatic and galvanodynamic polarization should be preferred in magnesium research [12,13]. The galvanostatic test allows charge control. It facilitates comparison of hydrogen evolution rates as different current densities pass through the sample. Birbilis et. al carried out a series of experiments comprising alternating galvanostatic and potentiostatic steps, in which a constant current density ensured anodic dissolution followed by polarization of the sample to a sufficiently negative potential and measurement of the cathodic current. Interestingly, the cathodic current increased after increasing anodic polarization [14].

Unfortunately, conventional electrochemical techniques lack spatial resolution and therefore provide little information on the local behavior at sites of corrosion initiation that occur within the range of nanometers and micrometers and to extract the electrochemical signal resulting from individual processes. For this purpose, two strategies have been undertaken: miniaturization of either the investigated sample by using microelectrodes [15] and microelectrode arrays [16], or the measuring cell [17,18]. In these cases, although the electrochemical signal represents an average of the entire exposed substrate, transients related to individual breakdown events or localized sites might be resolved above the background signal, allowing the various stages of the breakdown process to be resolved [15-19]. Yet, these methodologies require *ex situ* optical, electron or atomic force microscopies in order to correlate the electrochemical observations to specific features on the investigated sample [20-22]. Alternately, the use of scanning microelectrochemical techniques [23-25], in which electrodes of small dimensions are employed as sensing probes in near-field scanning configurations, leads to the synthesis of images where the pixels contain chemically and spatially resolved information on the electrochemical processes occurring at the surfaces under investigation. That is, the images are constructed from the individual results of the local electrochemical measurements. Although the successful application of SVET to the investigation of magnesium-based materials by Williams and coworkers has already been mentioned [6,9], the lack of chemical selectivity to identify the actual species participating in each site has driven the attention of researchers towards scanning electrochemical microscopy

(SECM). Despite the growing use of ion selective microelectrodes [26], amperometric detection remains the prevailing mode of SECM applied in the study of Mg corrosion [27,28]. The reduction potential of magnesium is beyond the reduction potential of water, preventing the redox conversion of some magnesium species to be employed for generation/collection modes in SECM. Thus, the monitoring of H_2 evolution is regarded to be the most accurate method for the measurement of the corrosion rate using the amperometric mode of the SECM [29], although the perturbation caused by vigorous hydrogen evolution has severely limited the application of this technique to investigate the corrosion of magnesium under polarization conditions [30].

A promising route to overcome the limited application of SECM for the investigation of magnesium under anodic polarization conditions was opened in Ref. [1] by employing a three-step (off-on-off) galvanic coupling operation sequence that effectively minimized the perturbation caused by hydrogen evolution on the current signal measured at the tip. The proof of concept was demonstrated using SECM analysis to investigate the role of the oxide layer formed on the surface of an aluminum-containing alloy, namely AZ63, in regards to the anomalous hydrogen evolution effect. It was shown that increased rates for hydrogen evolution were observed after the growth of the $Mg(OH)_2$ layer on the surface of AZ63. Since the eventual effect of aluminum and other alloying elements could not be discarded at that time, the new three-step polarization operation procedure for SECM was applied in this work for the analysis of 99.9% purity magnesium. In addition, the electrochemical activities of magnesium and AZ63 magnesium alloy were compared using the generator-collector mode of SECM under various experimental conditions.

2. Experimental

Metal strips of 99.9% grade magnesium supplied by Goodfellow (Cambridge, UK) were embedded in epoxy resin sleeve (EpofixKit, Struers, Denmark). The samples were abraded using wet abrasive paper (down to 4000 grit) and subsequently polished with alumina slurries down to 0.05 μm grain size. A small electrochemical cell was produced by placing at the bottom the Mg sample with the freshly polished surface facing up, and creating a small container for about 4 mL volume of the test electrolyte by wrapping Sellotape around the sample. Solutions were prepared from ultrapure water (Millipore water system, specific conductivity $\kappa = 5.6 \times 10^{-6}$ S cm^{-1} (Merck Millipore, Billerica, MS, USA) using sodium and potassium chlorides purchased from Reanal (Budapest, Hungary), and magnesium-chloride

hexahydrate and disodium ethylenediammin-tetraacetate (EDTA) from Merck (Darmstadt, Germany).

A Sensolytics SECM instrument (Bochum, Germany) was employed with Pt microelectrodes (ME) of 25 µm diameter and a ratio between the insulating shield thickness (*b*) to the disc electrode radius (*a*), *RG = b/a,* smaller than < 10 as tips (fabricated as described in Ref. [31]). The electrochemical cell was completed with an Ag/AgCl/(3 M) KCl reference electrode and a Pt auxiliary electrode. The tip-sample distance was adjusted at 20 µm by gently approaching the tip to the substrate under an optical microscope. Line and 2D-map scans were recorded at 25 µm s^{-1} scan rate.

3. Results and discussion

The potential of the Pt ME tip was set at -0.05 V vs. Ag/AgCl/(3 M) KCl to oxidize hydrogen as redox mediator for amperometric SECM operation. In this way, the actions of the corrosion product layer or any alloying element or impurity -which would function as a local cathode with respect to the magnesium matrix- could be studied in relation to the hydrogen evolution reaction (HER). Previous research using SECM has shown greater release of hydrogen gas from a surface covered with the dark layer of corrosion product that forms on magnesium in aqueous solutions containing chloride compared to the bare metal surface [1,8]. As sketched in **Figure 1**, these results were considered to suggest that the oxy-hydroxide layer exhibits catalytic properties for the corrosion of magnesium, either under spontaneous corrosion, at its corresponding open circuit potential (OCP) in the electrolyte, or under anodic polarization. These observations combine well with the observation of a net cathodic behavior of the oxide-coated surface when imaged using the scanning vibrating electrode technique (SVET) [6]. Since the rate of the HER does not always increase with layer thickness [1], the possible role of alloying materials and impurities was suggested instead. Noble impurities can accumulate on the dark corrosion layer, and HER might occur at increased rates even under potentials that are anodic for magnesium. This effect of surface enrichment is depicted in **Figure 2**. In fact, iron enrichment of the surface has been detected by scanning electron microscopy coupled with energy dispersive spectroscopy (EDS) [7]. Consequently, it has been proposed that with the advancement of the corrosion product front, the nobler iron particles or clusters can come into direct contact with the electrolyte promoting the formation of local cathodes. However, other studies have shown low enrichments in impurities during anodic polarization [32-33].

3.1. Effect of anodic polarization on hydrogen evolution

The effect of anodic polarization of the magnesium sample on hydrogen evolution rates was investigated by applying the following three-step (off-on-off) polarization routine to the magnesium sample immersed in naturally-aerated 1 mM NaCl solution. After 30 min immersion in the test electrolyte, a potential step at -1.0 V vs. Ag/AgCl/(3 M) KCl was applied to the sample for 30 min, and then it was left non-polarized and the electrolyte was stirred to remove the adherent bubbles on the sample. Although the open circuit potential of pure magnesium is ca. 0.2 V less negative than for the AZ63 alloy according to the Tafel plots shown in **Figure 3**, this potential value is well in the anodic range of both materials, and fast formation of a $Mg(OH)_2$ layer can be expected to occur during the anodic polarization step. Besides, this potential value may be employed to get information on the possible action of more noble elements on the electrochemical behavior of the oxy-hydroxide layers formed on the two magnesium-based materials.

Series of linear scans were measured along an arbitrarily chosen line through the metal every 5 min during the "off" steps as described in Ref. [1], which makes possible to compare the rate of hydrogen evolution before and after polarization. The line scans recorded before the polarization at -1.0 V vs. Ag/AgCl/(3 M) KCl are shown in **Figure 4A**, while **Figure 4B** shows those recorded after that polarization step. Although the current transients recorded after 5 min produce similar tip currents in both plots, the subsequent increase in H_2 evolution rates leads to the observation of higher currents after the polarization step at all remaining times. This fact can be better observed when the mean current values corresponding to the plateaus in the graphs are plotted as a function time in **Figure 5**. It should be noted that the current values recorded after 5 min were very close to each other due to the efficient removal of the adhered hydrogen bubbles formed during the polarization step, leaving only the H_2 formed during spontaneous corrosion conditions. However, after an additional 5 min there was a sharp increase in the rate of evolution of H_2 followed by a slow decrease for the remainder of the experiment. This abrupt change which occurs between 5 and 10 min was observed both before and after the polarization step, although the effect was greater for line scans recorded after the polarization step (namely, almost two times greater after the polarization). A slower decline after 10 min was found for line scans recorded after polarization. Although this finding was also observed in the case of the AZ63 alloy (see Figure 2 in Ref. [1]), the exponential decrease reported for the alloy could not be observed in the case of pure magnesium (note that the average tip currents are plotted in **Figure 5** while in the case of the alloy a logarithmic plot has been presented in Ref. [1]).

The observation of higher hydrogen evolution rates after anodic polarization step supports that the formation of the $Mg(OH)_2$ layer on the surface of the pure metal enhanced the hydrogen evolution rate on Mg. In addition, a certain passivating character of the oxide-covered surface must be considered to justify for the progressive decrease of the hydrogen evolution rates measured over longer times. This effect is particularly relevant in the case of the sample before anodic polarization because the corresponding decrease for the same surface after the polarization step is slower and extends over a longer period of time.

3.2. Effect of Mg^{2+} ion concentration on hydrogen evolution

Since the anodic polarization of a magnesium alloy may not only promote the formation of a magnesium oxide/hydroxide layer but also contain the oxides/hydroxides of alloying and other impurity metals, these more "noble" impurities are often invoked to account for the occurrence of the anomalous hydrogen evolution effect on magnesium-based materials. But from the comparison of the effect of anodic polarization on hydrogen evolution for 99.9% Mg and the AZ63alloy described in Section 3.1, it was shown that the enhanced HER described for this alloy in Ref. [1] also occurs on pure magnesium even in a greater extent. As result, this observation cannot be attributed to a surface enrichment of impurities, but to the formation of the $Mg(OH)_2$ layer that would have a catalytic effect for the HER despite certain passivating character. For this reason, an alternate experimental procedure was performed to enhance the formation of the $Mg(OH)_2$ layer consisting in the addition of Mg^{2+} ions to the electrolyte. As opposed to the anodic polarization routine described above, the addition of Mg^{2+} containing electrolyte should only result in the enhanced formation of the $Mg(OH)_2$ layer, but should have no significant effect on the growth of other metal oxides and hydroxides as they do not require the high alkaline pH values needed for the precipitation of the $Mg(OH)_2$ layer. On the other hand, the previous findings showed that there is a decay in the rate of the HER with time for both pure magnesium and the AZ63 alloy, a feature that was justified above by attributing a dual role to the Mg oxy-hydroxide bilayer, that is apart from the catalytic activity on the HER, and thus contribute to insulate the metal surface. To test this hypothesis, $MgCl_2$ solutions of two different concentrations were employed assuming that the less concentrated one (namely, 1 mM) would contribute to increase the rate of the HER, whereas the higher concentration (0.1 M) would produce the opposite effect. The experiments were repeated in NaCl solutions with identical Cl^- concentrations to those in the $MgCl_2$-containing solutions.

Figure 6A shows the distribution of H_2 evolution on pure magnesium immersed in 1 mM NaCl + 1 mM $MgCl_2$ solution. Due to the increased chloride concentration in the test solution, the experiments were also performed in 3 mM NaCl solution for comparison (see **Figure 6B**). Differences in the amounts of HER from the magensium samples immersed in the two electrolytes could be directly observed from the 2D maps. It was found that the hydrogen fluxes arising from magnesium increased significantly in the solution containing Mg^{2+} ions, as it would be expected if the oxy-hydroxide layer formed on magnesium were producing a catalytic effect for the HER. Since the same effect was observed for the AZ63 alloy in Figure 4 of Ref. [1], the behaviors of the alloy and pure magnesium were compared as it follows. Lines were selected from the 2D scans in which the tip crosses the sample and, similarly to the procedure followed with the line scans in **Figure 4A-B**, the current plateaus measured above the metals were averaged. In this way, a rough estimation was made for the hydrogen evolution rates, allowing the increases in the rate of the HER due to the addition of $MgCl_2$ to be compared for the two materials. Despite the rough estimation involved (that is, since the elapse of time during scan acquisition cannot be taken into consideration, the map is effectively regarded as an instantaneous image of the H_2 flux), a significant difference between the AZ63 alloy and the pure metal could be observed. In the case of the alloy, the addition of $MgCl_2$ caused an about 1.76 times higher hydrogen evolution rate, whereas the increase was 2.91 times for pure magnesium. The line scans also revealed a decay of the rate of the HER in time that was faster in the case of the alloy (cf. **Figure 5** with Figure 2 in Ref. [1]). It seemed that the oxides formed in the anodic dissolution partially insulate the magnesium surface.

In order to test this conclusion, a new series of line scans were performed above the pure magnesium in either 0.1 M $MgCl_2$ or 0.2 M NaCl solutions. This high concentration of Mg^{2+} would favor the fast formation of the $Mg(OH)_2$/MgO bilayer, and the insulator role was expected to be more pronounced than the catalytic effect. The line scans taken over both the Mg strip and the Mg alloy were recorded every 5 min for 40 min, and the average current values are plotted in **Figures 7A** and **7B**, respectively. In the case of the 0.1 M $MgCl_2$ solution the plateaus presented a rather smooth decay with time, although there was a small increase after 20 min (cf. **Figure 7A**). On the other hand, a greater fluctuation of the plateaus could be observed in the measurements performed in 0.2 M NaCl, and the decreasing tendency in the rate of the HER after 5 minutes could not be resolved unambiguously. It has also to be mentioned that in the presence of Mg^{2+} ions, the initial line scan shows more than 1.5 times higher HE rate than in 0.2 M NaCl. That is, initially the catalytic effect of the

$Mg(OH)_2$ layer can be clearly observed. Afterwards the decay in the HE rate seems to be faster in the presence of the high concentration of $MgCl_2$.

Although these findings seem to support our hypothesis, 2D scans were performed after 60 min immersion time to obtain the total distribution of hydrogen evolution on the pure magnesium. **Figure 8** shows the H_2 maps recorded in the two electrolytes. In a good agreement with the line scans, a higher H_2 flux was detected in the 0.2 M NaCl for both materials. That is, these maps exhibit the opposite behavior towards the HER with $MgCl_2$ addition to that previously described for the previous experiments with a smaller concentration of $MgCl_2$.

3.3. Effect of a complexing agent for Mg^{2+} ion on hydrogen evolution

The findings presented in the previous Sections have shown the effect produced on the rate of the hydrogen evolution by promoting the formation of the $Mg(OH)_2$ layer, and they were justified by proposing a dual role to this layer. At this stage, it seemed to be beneficial if a new approach were introduced to simplify the picture. That is, inasmuch that the formation of the catalytic layer is hindered, one would expect slower hydrogen evolution. The advantage of this approach is that we can exclude the thickness dependence from the overall impact of the layer. This is achieved by adding ethylene-diammine-tetraacetic acid (EDTA) as complexing agent to capture the Mg^{2+} ions released from the sample, thus preventing the precipitation of the oxide layer.

Figure 9 shows the 2D maps of H_2 evolution recorded over magnesium at its OCP. Significantly smaller hydrogen evolution rates can be observed when the solution contains the complexing agent. The decreased hydrogen generation rates occurring on the sample when the metal ions are complexed in the solution phase is indicated by the very weak and localized signal detected for hydrogen electroreduction in **Figure 9A**, despite using a more sensitive color scale in the graph compared to that employed for the map in the EDTA-free solution that is shown in **Figure 9B**. It can be concluded that by hindering the formation of the oxy-hydroxide layer, hydrogen evolution from the metal surface is greatly diminished, thus supporting that this layer would exhibit catalytic characteristics for HER as depicted in the sketch shown in **Figure 10A.** Although a slight pH change occurs when EDTA is added to the test electrolyte compared to the EDTA-free solution, and consequently HER would decrease due to such alkalization, the pH change is not sufficient to account for the observed changes, and this effect was neglected in the comparison.

Next, since it might be objected that the results shown in **Figure 9** were recorded without applying a polarization to the metal surface (i.e., effectively at the OCP in the corresponding electrolyte) and the electrical condition of the metal could be affected by the different composition of the electrolyte, and thus no adequately represent the characteristics of the surface film under anodic polarization, a new series of experiments was performed. In this case, the activity of the metal surface was monitored under both non-polarization and anodic polarization at -1.0 V Ag/AgCl/(3 M) KCl using the arrangement sketched in **Figure 10B**. For the sake of comparison, measurements were performed both in the absence and in the presence of EDTA in the electrolyte, and the obtained SECM maps are shown in **Figure 11**. It is observed that the application of an anodic polarization to magnesium always results in a significant enhancement of hydrogen evolution from the surface (cf. **Figures 11C** and **11A** for the EDTA-containing electrolyte, whereas **Figures 11D** and **11B** show the magnitude of the effect of anodic polarization for the metal immersed in the unmodified test solution). The impact of anodic polarization is greater when the complexing agent is not present in the electrolyte (see **Figure 11D**), but still significant in the case of the solution containing EDTA due to the contribution of anodic polarization to the formation of the oxy-hydroxide film effectively compensating for the opposing effect of complexation of the free metal ions (see **Figure 11C**). Therefore, we consider that our hypothesis is sustained.

4. Conclusions

In this paper a systematic study of the negative difference effect was presented for 99.9% magnesium, as well as the comparison with the behavior of AZ63 alloy under the same experimental conditions.

The results obtained with the amperometric SG-TC mode of the SECM supported the catalytic effect of the $Mg(OH)_2$/MgO bilayer, whereas the comparative experiments with pure Mg and the AZ63 alloy helped to separate the effect of the noble impurities from the catalytic effect. Greater hydrogen evolution rates were observed by facilitating the formation of the bilayer by adding an electrolyte containing the Mg^{2+} metal ions, whereas greatly depleted hydrogen evolution was observed when the Mg^{2+} ions where complexed using EDTA, thus effectively hindering the formation of the oxide layer. Similar trends were observed for pure magnesium as for the AZ63 alloy, although the latter contained Zn and Al elements that could contribute to the formation of the passive layer whereas becoming potential cathodes due to their more noble character comparted to magnesium.

Next, the experiments performed above pre-polarized and non-polarized magnesium and AZ63 provided additional new information on the hydrogen evolution reaction. Enhanced hydrogen evolution occurred on pre-polarized surfaces compared to the non-polarized ones, supporting that the formation of the oxy-hydroxide layer on magnesium leads to a catalytic effect for the HER in addition to its weak passivation characteristics.

Acknowledgements

D. Filotás expresses his greatest gratitude to the ERASMUS+ program for the financial support of a 2-month mobility grant to the University of La Laguna. B.M. Fernández-Pérez is grateful to the Canarian Agency for Research, Innovation and Information Society (Las Palmas de Gran Canaria, Spain) and the European Social Fund (Brussels, Belgium) for a research contract. Financial support by the Spanish Ministry of Economy and Competitiveness (MINECO, Madrid) and the European Regional Development Fund, under grant CTQ2016-80522-P, The National Research, Development and Innovation Office (Budapest, Hungary) under grant K125244, and the "Environmental industry related innovative trans- and interdisciplinary research team development in the University of Pécs knowledge base under SROP-4.2.2.D-15/1/Konv-2015-0015 project is gratefully acknowledged.

References

1. D. Filotás, B.M. Fernández-Pérez, L. Nagy, G. Nagy, R.M. Souto, A novel scanning electrochemical microscopy strategy for the investigation of anomalous hydrogen evolution from AZ63 magnesium alloy, Sensors and Actuators B-Chemical 308 (2020) 127691.
2. A.D. King, N. Birbilis, J.R. Scully, Accurate electrochemical measurement of magnesium corrosion rates: A combined impedance, mass-loss and hydrogen collection study, Electrochimica Acta 121 (2014) 394-406.
3. F. Cao, G.L. Song, A. Atrens, Corrosion and passivation of magnesium alloys, Corrosion Science 111 (2016) 835-845.
4. S. Thomas, N.V. Medhekar, G.S. Frankel, N. Birbilis, Corrosion mechanism and hydrogen evolution on Mg, Current Opinion in Solid State & Materials Science 19 (2015) 85-94.

5. M. Esmaily, J.E. Svensson, S. Fajardo, N. Birbilis, G.S. Frankel, S. Virtanen, R. Arrabal, S. Thomas, L.G. Johansson, Fundamentals and advances in magnesium alloy corrosion, Progress in Materials Science 89 (2017) 92-193.
6. G. Williams, N. Birbilis, H.N. McMurray, The source of hydrogen evolved from a magnesium anode, Electrochemistry Communications 36 (2013) 1-5.
7. M. Taheri, J.R. Kish, N. Birbilis, M. Danaie, E.A. McNally, J.R. McDermid, Towards a physical description for the origin of enhanced catalytic activity of corroding magnesium surfaces, Electrochimica Acta 116 (2014) 396-403.
8. S.H. Salleh, S. Thomas, J.A. Yuwono, K. Venkatesan, N. Birbilis, Enhanced hydrogen evolution on $Mg(OH)_2$ covered Mg surfaces, Electrochimica Acta 161 (2015) 144-152.
9. G. Williams, N. Birbilis, H.N. McMurray, Controlling factors in localized corrosion morphologies observed for magnesium immersed in chloride containing electrolyte, Faraday Discussions 180 (2015) 313-330.
10. D. Höche, C. Blawert, S.V. Lamaka, N. Scharnagl, C. Mendis, M.L. Zheludkevich, The effect of iron re-deposition on the corrosion of impurity-containing magnesium, Physical Chemistry Chemical Physics 18 (2016) 1279-1291.
11. J. Yang, C. Blawert, S.V. Lamaka, K.A. Yasakau, L. Wang, D. Laipple, M. Schieda, S. Di, M.L. Zheludkevich, Corrosion inhibition of pure Mg containing a high level of iron impurity in pH neutral NaCl solution, Corrosion Science 142 (2018) 222-237.
12. G.S. Frankel, A. Samaniego, N. Birbilis, Evolution of hydrogen at dissolving magnesium surfaces, Corrosion Science 70 (2013) 104-111.
13. A. Samaniego, N. Birbilis, X. Xia, G. S. Frankel, Hydrogen evolution during anodic polarization of Mg alloyed with Li, Ca, or Fe, Corrosion 71 (2015) 224-233.
14. N. Birbilis, A.D. King, S. Thomas, G.S. Frankel, J.R. Scully, Evidence for enhanced catalytic activity of magnesium arising from anodic dissolution, Electrochimica Acta 132 (2014) 277-283.
15. P.C. Pistorius, G.T. Burstein, Metastable pitting corrosion of stainless steel and the transition to stability, Philosophical Transactions of the Royal Society London A 341 (1992) 531-559.
16. Y. Tan, Sensing localised corrosion by means of electrochemical noise detection and analysis, Sensors and Actuators B-Chemical 139 (2010) 688-698.
17. T. Suter, H. Böhni, A new microelectrochemical method to study pit initiation on stainless steels, Electrochimica Acta 42 (1997) 3275-3280.

18. V. Vignal, H. Krawiec, O. Heintz, R. Oltra, The use of local electrochemical probes and surface analysis methods to study the electrochemical behaviour and pitting corrosion of stainless steels, Electrochimica Acta 52 (2007) 4994-5001.
19. R.K. Gupta, N.L. Sukiman, M.K. Cavanaugh, B.R.W. Hinton, C.R. Hutchinson, N. Birbilis, Metastable pitting characteristics of aluminium alloys measured using current transients during potentiostatic polarisation, Electrochimica Acta 66 (2012) 245-254.
20. F.A. Martin, C. Bataillon, J. Cousty, In situ AFM detection of pit onset location on a 304L stainless steel, Corrosion Science 50 (2008) 84-92.
21. N. Birbilis, K. Meyer, B.C. Muddle, S.P. Lynch, In situ measurement of corrosion on the nanoscale, Corrosion Science 51 (2009) 1569-1572.
22. V. Maurice, P. Marcus, Passive films at the nanoscale, Electrochimica Acta 84 (2012) 129-138.
23. R.S. Lillard, Scanning electrode techniques for investigating near-surface solution current densities, in: Analytical Methods in Corrosion Science and Engineering, P. Marcus, F. Mansfeld (Eds.); CRC Press, Boca Raton, FL, 2006, pp. 571-604.
24. M.B. Jensen, D.E. Tallman, Application of SECM to corrosion studies, in Electroanalytical Chemistry: A Series of Advances, Vol. 24, A.J. Bard, C. Zoski (Eds.); CRC Press, Boca Raton, FL, 2012, pp. 171-286.
25. N.A. Payne, L.I. Stephens, J. Mauzeroll, The application of scanning electrochemical microscopy to corrosion research, Corrosion 73 (2017) 759-780.
26. J. Izquierdo, A. Kiss, J.J. Santana, L. Nagy, I. Bitter, H.S. Isaacs, G. Nagy, R.M. Souto, Development of Mg^{2+} ion-selective microelectrodes for potentiometric scanning electrochemical microscopy monitoring of galvanic corrosion processes, Journal of The Electrochemical Society 160 (2013) C451-C459.
27. S. Thomas, J. Izquierdo, N. Birbilis, R.M. Souto, Possibilities and limitations of scanning electrochemical microscopy of Mg and Mg alloys, Corrosion 71 (2015) 171-183.
28. P. Dauphin-Ducharme, J Mauzeroll, Surface analytical methods applied to magnesium corrosion, Analytical Chemistry 87 (2015) 7499-7509.
29. S.S. Jamali, S.E. Moulton, D.E. Tallman, M. Forsyth, J. Weber, G.G. Wallace, Applications of scanning electrochemical microscopy (SECM) for local characterization of AZ31 surface during corrosion in a buffered media, Corrosion Science 86 (2014) 93-100.
30. J. Izquierdo, B.M. Fernández-Pérez, D. Filotás, Z. Őri, A. Kiss, R.T. Martín-Gómez, L. Nagy, G. Nagy, R.M. Souto, Imaging of concentration distributions and hydrogen

evolution on corroding magnesium exposed to aqueous environments using scanning electrochemical microscopy, Electroanalysis 28 (2016) 2354-2366.

31. C. Kranz, M. Ludwig, H.E. Gaub, W. Schuhmann, Lateral deposition of polypyrrole lines by means of the scanning electrochemical microscope, Advanced Materials 7 (1995) 38-40.
32. N. Birbilis, T. Cain, J.S. Laird, X. Xia, J.R. Scully, A.E. Hughes, Nuclear microprobe analysis for determination of element enrichment following magnesium dissolution, ECS Electrochemical Letters 4 (2015) C34-C37.
33. D. Lysne, S. Thomas, M.F. Hurley, N. Birbilis, On the Fe enrichment during anodic polarization of Mg and its impact on hydrogen evolution, Journal of The Electrochemical Society 162 (2015) C396-C402.

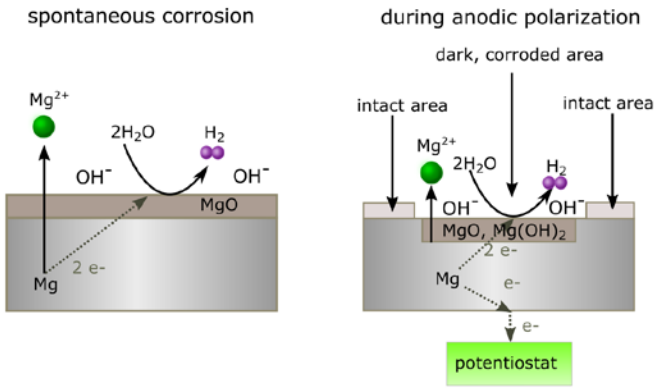

Figure 1. Schemes of the spontaneous magnesium corrosion (left) and the corrosion during anodic polarization (right) according to the enhanced catalytic surface theory**.**

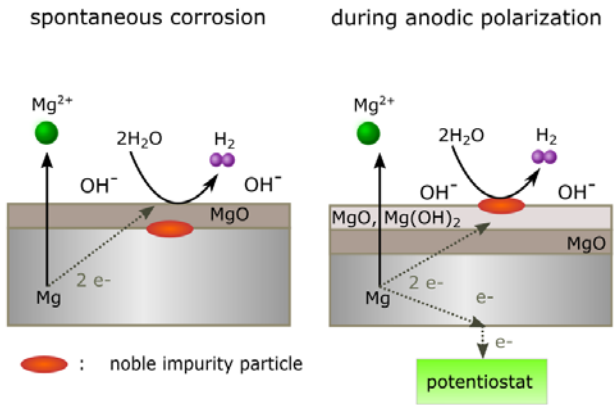

Figure 2. Schemes of the anomalous hydrogen evolution invoking a surface enrichment of noble impurities in the case of spontaneous magnesium corrosion (left) and the corrosion during anodic polarization (right).

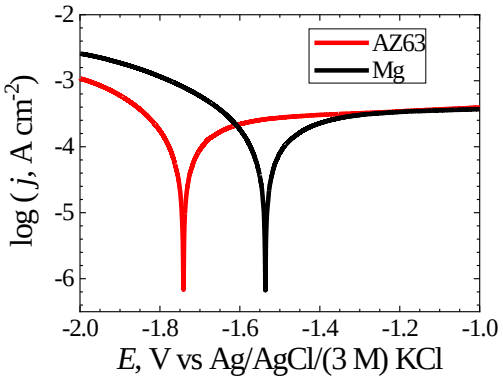

Figure 3. Potentiodynamic polarization curves recorded for 99.9% Mg (black) and AZ63 alloy (red) in 1 mM NaCl. Scan rate: 5 mV s^{-1}.

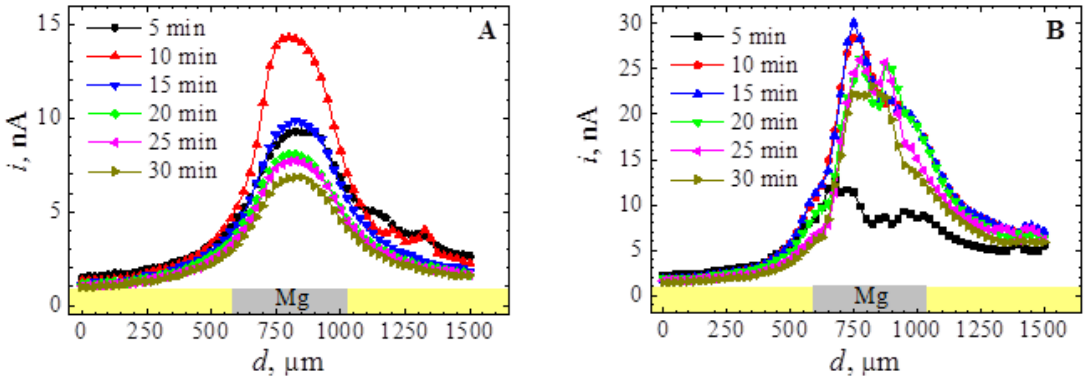

Figure 4. Line scans recorded over a 99.9% magnesium sample immersed in 1 mM NaCl solution for different times before (A) and after (B) application of an anodic polarization (30 min at E_{sample} = -1.0 V vs. Ag/AgCl/(3 M) KCl). No polarization was applied to the Mg sample during the SECM operation. Tip: Pt, 25 µm diameter, RG < 10; E_{tip} = -0.05 V vs. Ag/AgCl/(3 M) KCl; tip-sample distance: 20 µm; scan rate: 25 µm s^{-1}.

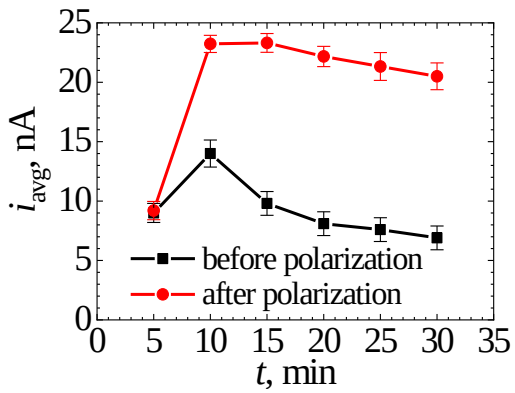

Figure 5. Average H_2 fluxes determined from the current transients recorded over magnesium in Figure 4A-B before and after application of an anodic polarization using the "off-on-off" sequence.

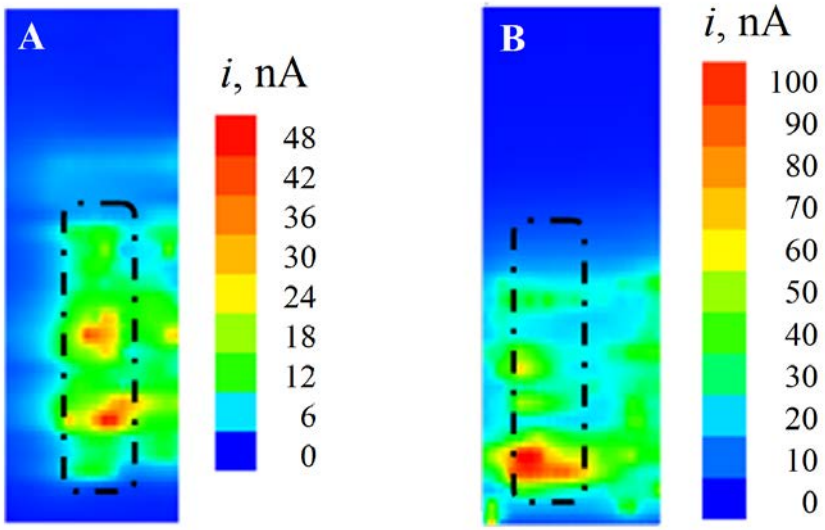

Figure 6. 2D maps recorded over a magnesium strip (0.3 × 1.5 mm^2) immersed for 40 min in: (A**)** 1 mM NaCl + 10 mM EDTA, and (B) 1 mM NaCl solutions. Images represent an area of 1000 × 3000 μm^2. Samples were left unbiased. Tip: Pt, 25 µm diameter, RG < 10; E_{tip} = -0.05 V vs. Ag/AgCl/(3 M) KCl; tip-sample distance: 20 µm; scan rate: 25 µm s^{-1}.

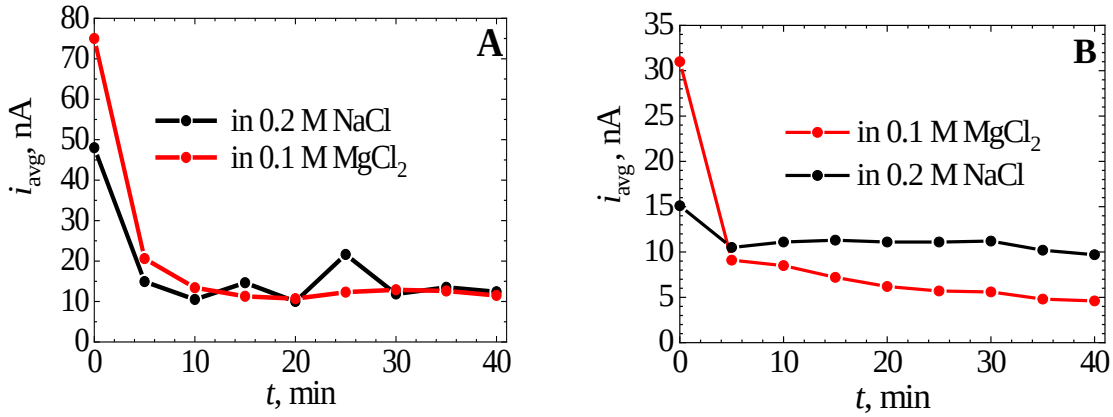

Figure 7. Average H_2 fluxes determined from the current transients recorded over: (A) pure Mg, and (B) AZ63 alloy samples immersed in the indicated electrolytes. No polarization was applied to the samples during the SECM operation.

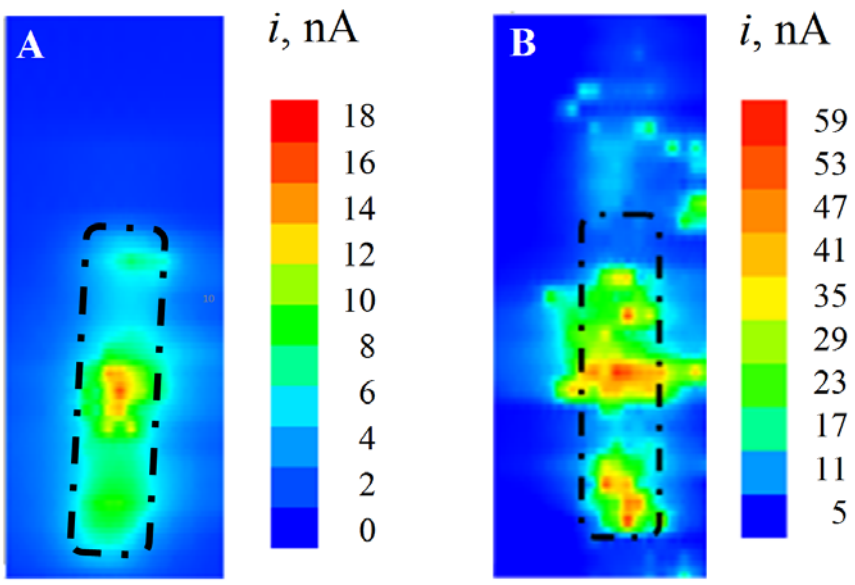

Figure 8. 2D maps recorded over a magnesium strip (0.3 × 1.5 mm^2) immersed for 60 min in: (A**)** 0.1 M $MgCl_2$, and (B) 0.2 M NaCl solutions. Images represent an area of 1000 × 3000 μm^2. Samples were left unbiased. Tip: Pt, 25 µm diameter, RG < 10; E_{tip} = -0.05 V vs. Ag/AgCl/(3 M) KCl; tip-sample distance: 20 µm; scan rate: 25 µm s^{-1}.

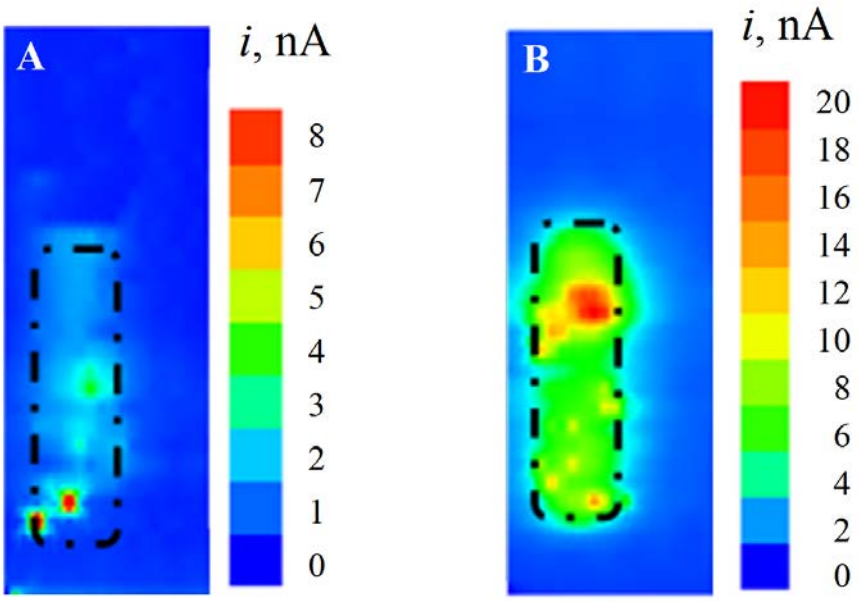

Figure 9. 2D maps recorded over a magnesium strip (0.3 × 1.5 mm^2) immersed for 60 min in: (A**)** 1 mM NaCl + 10 mM EDTA, and (B) 1 mM NaCl solutions. Images represent an area of 950 × 3000 μm^2. Samples were left unbiased. Tip: Pt, 25 µm diameter, RG < 10; E_{tip} = -0.05 V vs. Ag/AgCl/(3 M) KCl; tip-sample distance: 20 µm; scan rate: 25 µm s^{-1}.

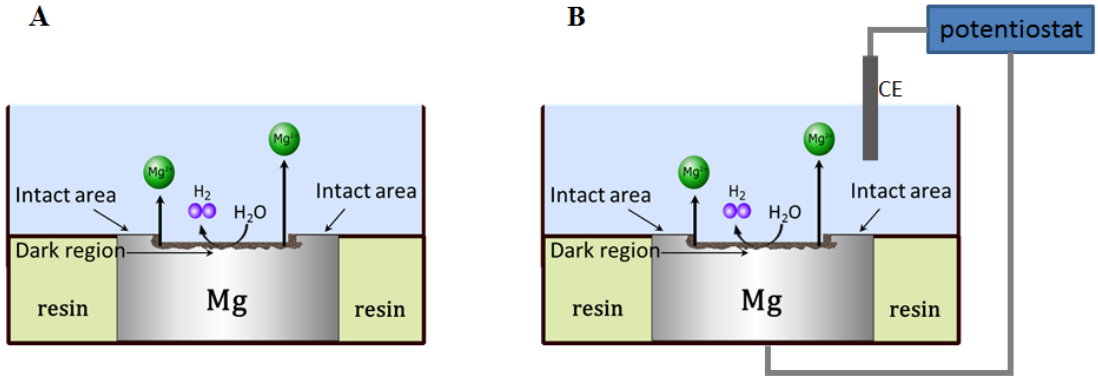

Figure 10. Sketches describing the catalytic effect of the oxy-hydroxide layer formed on the surface of magnesium under (A) OCP conditions, and (B) anodic polarization using a potentiostat.

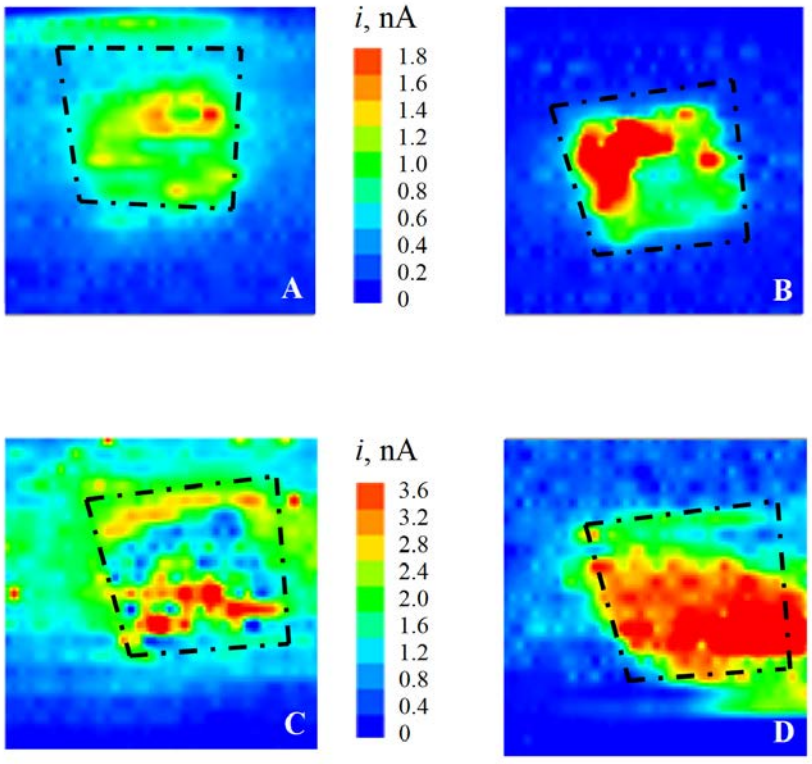

Figure 11. 2D maps recorded over a magnesium strip (1.5 × 1.5 mm^2) immersed for 60 min in: (A,C**)** 1 mM NaCl + 10 mM EDTA, and (B,D) 1 mM NaCl solutions. Images represent an area of 2000 × 2000 μm^2. Samples were: (A,B) left unbiased, and (C,D) anodically polarized at -1.0 V Ag/AgCl/(3 M) KCl. Tip: Pt, 25 µm diameter, RG < 10; E_{tip} = -0.05 V vs. Ag/AgCl/(3 M) KCl; tip-sample distance: 20 µm; scan rate: 25 µm s^{-1}.